Comparison of Rain Gauge Network and Weather Radar Data: Case Study in Angra dos Reis, Brazil

Elton John Robaina da Silva [1], Camila Nascimento Alves [1,2], Priscila Celebrini de Oliveira Campos [1], Raquel Aparecida Abrahão Costa e Oliveira [1], Maria Esther Soares Marques [1], José Carlos Cesar Amorim [1] and Igor Paz [1,*]

1   Instituto Militar de Engenharia, Praça General Tibúrcio 80, Praia Vermelha, Rio de Janeiro 22290-270, Brazil
2   Faculdade de Ciências e Tecnologia, Universidade Federal do Pará, Tv. We Vinte e Seis, 02—Coqueiro, Ananindeua 67130-660, Brazil
*   Correspondence: igorpaz@ime.eb.br

Abstract: This paper presents a comparison between rain gauge network and weather radar data in Angra dos Reis city, located in the State of Rio de Janeiro (RJ), Brazil. The city has a high incidence of natural disasters, especially associated with heavy rains in densely populated areas. In this work, weather radar data with a spatial resolution of 1 km were obtained from dual-polarimetric S-band radar operated by the Environmental State Institute of Rio de Janeiro (INEA), located in the Guaratiba neighborhood in Rio de Janeiro city, Brazil; the rain gauge measurements were provided by the National Center for Monitoring and Warning of Natural Disasters (CEMADEN), which is composed of a network with 30 rain gauges covering the studied area. The comparison between the two datasets enables the analysis of which radar products better fit the rain gauge network's accumulated rainfall by quantifying the uncertainties in precipitation estimates at radar pixels where rain gauges are located. The results indicated that radar products generated with the help of regression techniques obtained from the relation between radar reflectivities and rain gauge measurements were a better fit, constituting essential information while dealing with efficient regulation for rainfall monitoring and forecasting to minimize the risks associated with extreme events.

Keywords: rain gauge network; spatiotemporal variability; S-band radar; extreme events

1. Introduction

The vulnerability of urban areas to extreme events, particularly heavy rainfall, is a known and widely discussed problem [1–5]. The global increases in urbanization and population density in these areas, which are characterized by high levels of imperviousness and shorter response times, require an improvement in their capacities to adapt to climate change [6–10] and to better measure and model hydro-meteorological events [11–13].

Thus, there is great interest in assessing the reliability and spatiotemporal resolution of the available data. In the case of obtaining urban catchment-scale rainfall data, two sensors are mostly used: rain gauges and weather radars [14,15]. Rain gauges provide local rainfall measurements, which are relatively accurate albeit unable to cover large areas with dense networks and therefore limited in assessing the spatial rainfall variability [15–19]. On the other hand, weather radars provide spatiotemporal rainfall estimates by surveying large areas and have thus been used to address the sparseness of rain gauge networks [20–22].

Nevertheless, these weather radar estimates are not direct rainfall measurements such as those provided by rain gauges. Weather radars perform reflectivity measurements, from which rainfall intensities are indirectly obtained. This process has intrinsic uncertainties [23]. To cope with these uncertainties, some corrections have been applied [24]. In particular, for high rainfall intensities, dual-polarization technology exploring the flatness of large raindrops has been employed with the help of the specific differential phase (KDP) [25–29].

The goal of this study was to perform a comparison between rain gauge network and weather radar data in Angra dos Reis city, Brazil. The rain gauge measurements were provided by the National Center for Monitoring and Warning of Natural Disasters (CEMADEN), which is composed of a network with 30 rain gauges covering the studied area. The weather radar data were the result of dual-polarimetric S-band radar (operated by the Environmental State Institute of Rio de Janeiro—INEA [30]) located in the Guaratiba neighborhood (with an average distance of approximately 70 km from Angra dos Reis) in Rio de Janeiro city, Brazil. Thus, with this comparison, we analyzed which of Guaratiba's S-band radar products better fit the rain gauge network's accumulated rainfall by quantifying the uncertainties in precipitation estimates at radar pixels where rain gauges are located. This is especially important to cope with the well-known difficulty of rain gauge network sparseness [15,19,22]. Being able to estimate rainfall in ungauged areas with the help of weather radars would help decision-makers to improve rainfall monitoring and forecasting, minimizing the risks associated with extreme events.

To achieve these objectives, this paper is structured as follows: the second section presents the case study description, rainfall data (obtained from rain gauge network and S-band radar), the description of different radar products, the studied rainfall events, and the statistical methods used to analyze the rainfall data comparison; the third section presents the results; and finally, the fourth section presents the discussion and final considerations.

2. Materials and Methods

2.1. Case Study Area

Angra dos Reis is located in the southern region of the State of Rio de Janeiro, Brazil (Figure 1). It is an 813.420 km² semi-urbanized area with an estimated population of 210,171 inhabitants in 2021 [31], and it is located near an important nuclear power plant. The region is situated in the context of the geomorphological domain of the escarpments of Serra do Mar/Serra da Bocaina. The escarpments of Angra dos Reis are notable for having steep faces facing the ocean, alternating with embedded river valleys. The geology of the site is composed of igneous and metamorphic rocks of the Mesoproterozoic and Neoproterozoic ages, as well as orogenic and post-orogenic granites [32]. The city is crossed by torrential rivers with a torrential regime, grouping rivers into those that originate on the slopes of the Serra do Mar or on the top of the plateau and its tributaries, which flow into the Ilha Grande Bay [33].

Urbanization in the region has developed on slopes susceptible to shallow landslides induced by heavy rainfall. Between 2016 and 2018, the municipality recorded 52 occurrences of landslides, according to Civil Defense data [34]. It is noteworthy that, as in several other Brazilian municipalities, the municipality of Angra dos Reis has undergone an intense and disorderly process of urbanization, negatively affecting its sustainable development [35].
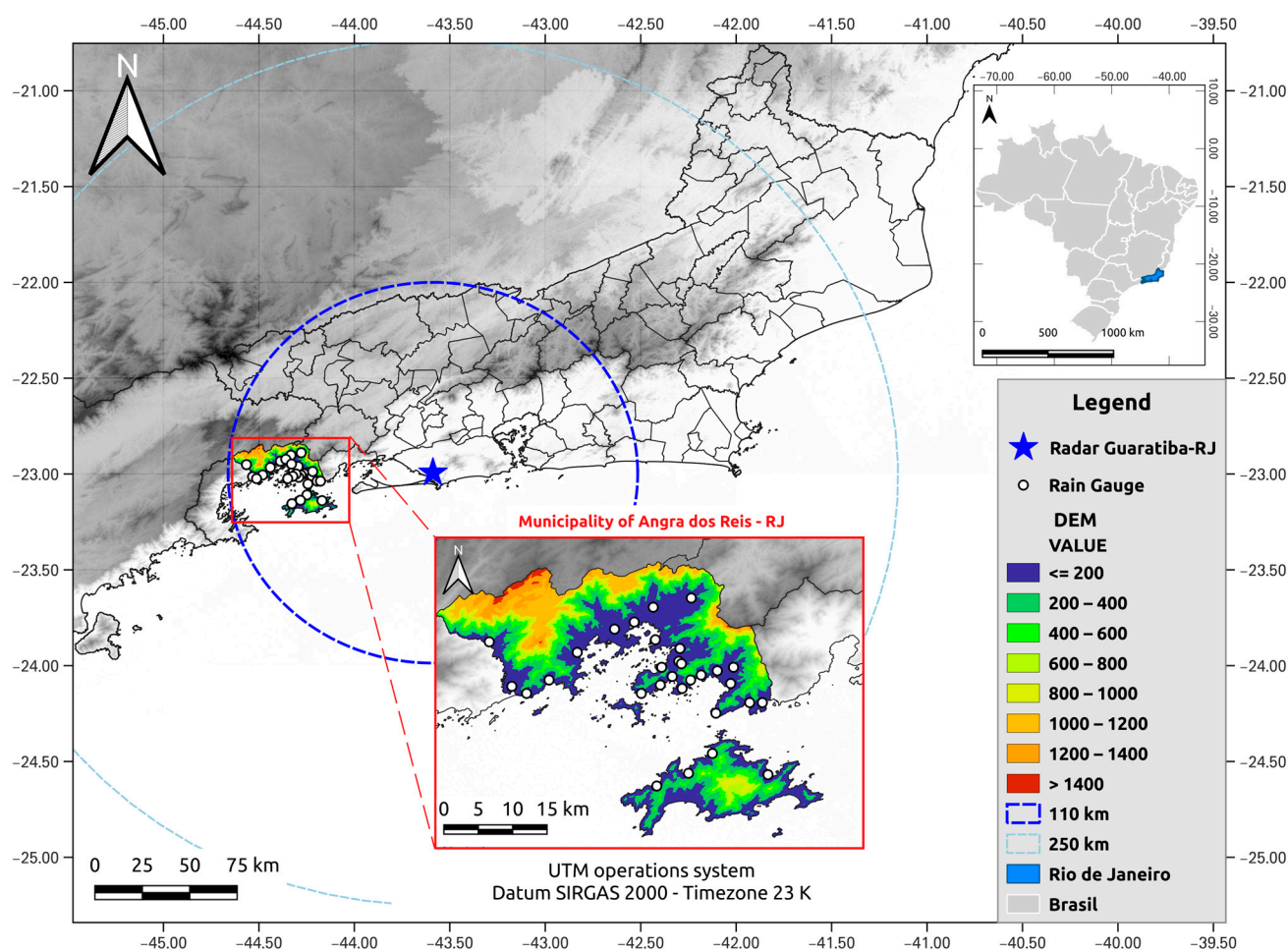
Figure 1. Locations of the rain gauge network of the municipality of Angra dos Reis (RJ) and of Guaratiba's S-band radar in the state of Rio de Janeiro, Brazil.

2.2. Rainfall Data

2.2.1. Rain Gauge Data

Rainfall data were obtained from the National Center for Monitoring and Warning of Natural Disasters (CEMADEN). The CEMADEN rain gauge network is composed of automatic rain gauges, which are connected to CEMADEN servers and transmit cumulative rainfall measurements in millimeters every 10 min. In periods where no rain is observed, rain gauges are configured to send an accumulated value of zero millimeters every 60 min. For this work, data from 30 rainfall stations located in the municipality of Angra dos Reis (RJ) were used (Figure 1 and Table 1).

The rain gauge network data are verified by an activity control system developed by CEMADEN, which identifies faults and filters the data generated by faulty equipment. The rainfall data are then made available without undergoing any further processing.

The rain gauges located in the city of Angra dos Reis were mostly distributed according to what the World Meteorological Organization (WMO) recommends for local-scale and mesoscale forecasting [36] and were located at distances of 3 km to 100 km from each other, mainly covering the coastal region. Nevertheless, the sparseness of the rain gauges' distribution is a major limitation on the network's ability to cover the entire territory of the region.

Table 1. Identification, station name, and geographic coordinates of the 30 studied rain gauges.

ID	Station Name	Lat	Lon
P1	Angra dos Reis	−22.9785	−44.2958
P2	Areal	−22.9820	−44.2920
P3	Ariró	−22.9020	−44.3320
P4	BNH	−22.9920	−44.2410
P5	Bracuí	−22.9330	−44.3870
P6	Camorim	−22.9980	−44.2640
P7	Camorim Pequeno	−23.0050	−44.2790
P8	Enseada	−22.9870	−44.3200
P9	Frade	−22.9660	−44.4400
P10	Itanema	−22.9230	−44.3590
P11	Manbucaba	−22.9510	−44.5650
P12	Mombaça	−23.0170	−44.2910
P13	Monsuaba	−23.0100	−44.2220
P14	Monsuaba 2	−22.9870	−44.2180
P15	Parque do Belém	−22.9604	−44.2941
P16	Parque Perequê	−23.0140	−44.5330
P17	Ponta Leste	−23.0520	−44.2430
P18	Pontal	−22.9480	−44.3290
P19	Portogalo	−23.0370	−44.1950
P20	Praia Brava	−23.0050	−44.4800
P21	Praia da Chacara	−23.0000	−44.3050
P22	Praia das Goiabas	−23.0240	−44.5120
P23	Praia de Araçatiba	−23.1550	−44.3270
P24	Praia de Bananal	−23.1090	−44.2480
P25	Praia de Garatucaia	−23.0370	−44.1770
P26	Praia Sitio Forte	−23.1370	−44.2820
P27	São Bento	−23.0120	−44.3220
P28	Serra d'Água	−22.8890	−44.2780
P29	Vila do Abraão	−23.1390	−44.1690
P30	Vila Velha	−23.0240	−44.3490

2.2.2. Radar Data

The State of Rio de Janeiro (RJ) has two dual-polarization S-band Doppler weather radars operated by the Environmental State Institute of Rio de Janeiro (INEA), located in the region of Guaratiba in Rio de Janeiro−RJ (Lat: −22°59′35.81077″ S; Lon: −43°35′16.65427″ W; Orthometric Height: 114.273 m + 4.35 m (tower floor) + 4.5 m (pedestal) ~ 123m) and in Macaé−RJ city (Lat: −22°24′20.99917″ S; Lon: −41°51′37.65632″ W; Orthometric Height: 72.867 m + 4 m (tower floor) + 4.5 m (pedestal) ~ 81 m). The equipment is currently configured to perform seven scans at different elevations (ranging from 0.5° to 7.5°) every 5 min. These radars can estimate the amount of rain within a radius of approximately 250 km and a rain intensity up to 480 km. The implementation of this equipment officially took place in February 2015, and the characteristics of its systems are summarized in Table 2.

In this study, only Constant-Altitude Plan Position Indicator (CAPPI) products [37,38] at 2 km height with a spatial resolution of 1 km, obtained from Guaratiba's S-band radar data, in scans of 5 and 10 min were used. The capture height value was considered, assuming that precipitation measured above the surface takes 3 to 10 min to fall and that convective rains tend to persist due to their evolutionary nature [37].

The CAPPI product was determined by converting the value of a radar field to a grid point. The procedure is performed by interpolating the points collected within a given radius of action and weighting these points close to the range of points on the grid by the Barnes method [39]. In addition, filters are applied according to various criteria for removing unwanted points in interpolation [39–41]. Although the Cressman filter [42] has been widely used for Spatial Objective Analysis (SOA), the Barnes filter is preferable due to the ease of calculating the response function [43]. The Barnes method is widely used in

geospatial sciences to reshape data values recorded at points distributed in a representative analytical field [44].

Table 2. Characteristics of dual-polarization S-band Doppler weather radars located in the State of Rio de Janeiro, Brazil, operated by INEA.

Parameter	Dual-Polarization S-Band Doppler Radar
Transmitter	2.8 GHz
Pulse Repetition Frequency (PRF)	600 Hz
Pulse width	1μsec
Pulse Repetition Time (PRT)	1.67 ms
Peak power	≥750 kW
Antenna gain, horizontal and vertical	45 dB
Antenna aperture	8.5
Beam width horizontal and vertical	1°
Polarimetric mode	STSR [1]
Nyquist Velocity	48.195 m/s
Number of samples used to compute moments	60
Radar Receiver Bandwidth	1 MHz
Radar Transmit Power Horizontal and Vertical Channel	800 watts
Scan mode	Plan Position Indicator (PPI)
Radial range	250 km
Radar fields [2]	UH, UV, DBZH, DBZV, ZDR, RHOHV, PHIDP, NCPH, NCPV, SNRHC, SNRVC, VELH, VELV, WIDTHH, WIDTHV, CCORH, CCORV

Notes: [1] Simultaneous Transmission and Simultaneous Reception; [2] UH is Unfiltered Reflectivity Factor H, UV is Unfiltered Reflectivity Factor V, DBZH is Equivalent Reflectivity Factor H, DBZV is Equivalent Reflectivity Factor V, ZDR is Log Differential Reflectivity H-V, RHOHV is Cross-Correlation Ratio H-V, PHIDP is Differential Phase H-V, NCPH is Normalized Coherent Power H, NCPV is Normalized Coherent Power V, SNRHC is Signal-to-Noise Ratio Co-polar H, SNRVC is Signal-to-Noise Ratio Co-polar V, VELH is Radial Velocity H, VELV is Radial Velocity V, WIDTHH is Doppler Spectrum Width H, WIDTHV is Doppler Spectrum Width V, and CCORH is Clutter Correction H, CCORV is Clutter Correction V.

Radar reflectivity (*Z*) can be converted into precipitation intensity (*R*) through several empirical relationships, often called *Z-R* equations [45–47].

$$Z[\text{dBZ}] = a\left(R\left[\text{mm·h}^{-1}\right] \right)^{b} \tag{1}$$

where a and *b* are experimentally determined constants that are related to the drop size distribution (DSD) in the atmosphere and radar reflectivity. DSD varies with the type and phase of precipitation (solid or liquid) and also depends on geographic location, altitude, and spatial exposure [48].

Through the introduction of double polarization in meteorology by weather radars [49], significant improvements could be achieved in rain measurements. The effectiveness of the use of dual-polarization radar for quantitative precipitation estimation (QPE) has been demonstrated by several previous studies [47,50,51]. Significant advantages have been observed in rainfall estimates using combinations of reflectivity (*Z*), differential reflectivity (Z_{DR}), and the specific differential phase (K_{DP}) compared to traditional methods (*Z-R*). The use of Z_{DR} in combination with *Z* allows the mitigation of uncertainties related to DSD variability, while K_{DP}-based methods are less sensitive to DSD variations and are immune to radar calibration errors, partial beam blocking, and attenuation by precipitation or a wet radome [27,47,52]. Thus, a typical solution for S-band radars is a combination of an $R(K_{DP})$ relationship for higher rainfall rates and an $R(Z,Z_{DR})$ relationship for lower rainfall rates, where K_{DP} becomes noisier and more susceptible to DSD [53]. A similar combination for the determination of rain products was used by Paz et al. [17] in their research on the Bièvre river basin.

In this work, the specific differential phase (K_{DP}) was calculated based on the variational method described by Maesaka et al. [54]. The authors identified that classical methods such as iterative filtering and local linear regression [55] may also estimate a negative K_{DP} in the rain, although the positive value is expected for pure raindrops, which generates problems in rain estimation and the correction of attenuation [37,54]. The estimation method of the proposed K_{DP} considers a monotonically increasing differential phase of propagation, where the differential phase Φ_{DP} (named PHIDP in Table 2) increases as the radar range is limited to rain below the melting layer and/or hot clouds at weather radar frequencies. The K_{DP} estimated by this method always assumes a positive value. The methodology can only be applied to radar data with a constant range resolution, being considered a sophisticated processing technique by Ryzhkov and Zrnic [56].

$$K_{DP} = \frac{1}{2} \frac{\partial \Phi_{DP}}{\partial r} \tag{2}$$

where r is the range.

In addition to these traditional relationships, methods combined with specific attenuation (A) have also been explored due to the low sensitivity of the $R(A)$ relationship to the variability in DSD [53,57].

Specific attenuation (A) was obtained from the ZPHI method proposed by Testud et al. [58]. The method aims to correct radar-derived data as a function of attenuation, taking into account the variability in the drop size distribution (DSD) in the rainfall estimate [59]. Ryzhkov et al. [53] demonstrated that the use of attenuation for rainfall estimates is even more promising on S-band radars when compared to shorter-wavelength radars, since the specific attenuation is immune to reflectivity biases caused by incorrect radar calibration and partial beam block and effects caused by a wet radome, and $R(A)$ is also immune to these factors. In addition, Le Bouar et al. [60] demonstrated significant advantages of the use of this method in relation to classical Z-R methods that do not take into account the attenuation.

The specific attenuation (A) is calculated from the radial profile of the attenuated reflectivity (Z_a) and the differential phase Φ_{DP} between intervals r_1 and r_2, where r_1 is the first gate that contains precipitation, and r_2 is the last gate or gate immediately below the bottom of the melting layer. In the case of dual-polarization radars, the plane-integrated attenuation (PIA) is estimated using the full extent of the differential phase Φ_{DP} along the way to spread the rain $\Delta\Phi_{DP}$ [53,58,61–63].

$$A(r) = \frac{[Z_a(r)]^\beta C(\beta, PIA)}{I_a(r_1, r_2) + C(\beta, PIA) I_a(r, r_2)} \tag{3}$$

where

$$PIA = \alpha \Delta\Phi_{DP}, \ PIA(r_1, r_2) = \alpha[\Phi_{DP}(r_2) - \Phi_{DP}(r_1)] \tag{4}$$

$$I_a(r_1, r_2) = 0.46\beta \int_{r_1}^{r_2} [Z_a(s)]^\beta ds \tag{5}$$

$$I_a(r, r_2) = 0.46\beta \int_{r}^{r_2} [Z_a(s)]^\beta ds \tag{6}$$

$$C(\beta, PIA) = exp(0.23 \ \beta \ PIA) - 1 \tag{7}$$

where α is the net ratio between A and K_{DP} over the radius at a given temperature, β is a constant exponent that usually varies between 0.6 and 0.9 at microwave frequencies, and Z_a represents the measured radar reflectivity that is not corrected by calibration and attenuation, expressed as a linear scalar [53].

Statistical studies performed by Cocks et al. [57] using S-band radar for different types of rain found that for continental rainfall events, α is on average 0.018 deg^{-1}, and for tropical rainfall events, α is on average 0.028 deg^{-1}. These results are similar to the values of α reported by Ryzhkov et al. [53], who used α values of 0.02–0.03 deg^{-1} for high-quality

rainfall estimates in most areas of Hurricane Irene and 0.008–0.015 deg^{-1} for the Oklahoma flood case. In this study, we used 0.02 deg^{-1} as the value of α, and β was set to 0.64884 according to Helmus and Collis [41], a value similar to that used by [53,62,63] (0.62). It is noteworthy that, in this study, the product generated from the reflectivity corrected by the attenuation [64] through the ZPHI methodology was used for comparative purposes with the reflectivity of the equipment under study without any correction. Figure 2 illustrates a comparison between Guaratiba's radar reflectivity without (Figure 2a) and with the ZPHI-method correction (Figure 2b).
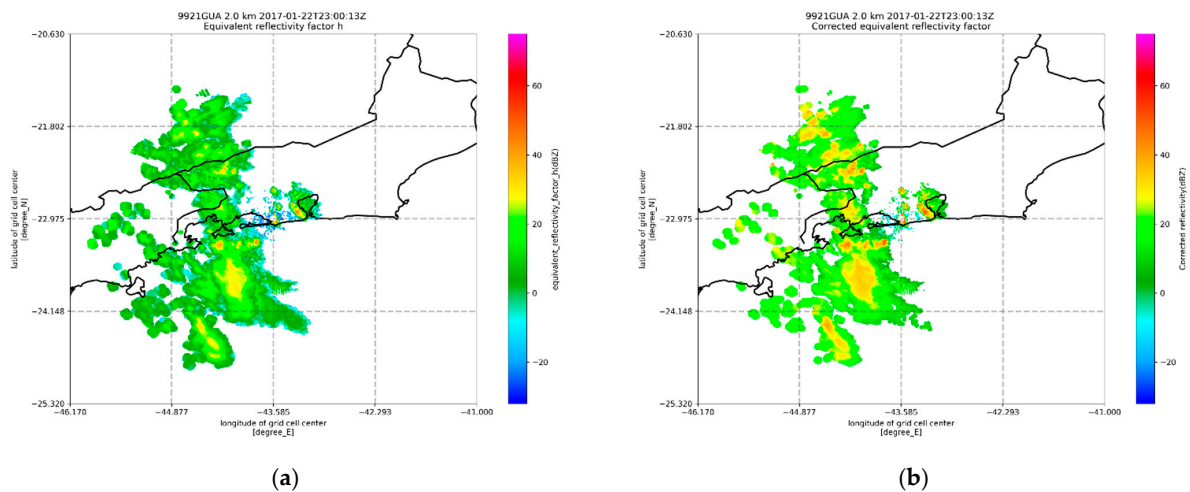

(a)   (b)

Figure 2. Illustration of different products of Guaratiba's S-band radar reflectivity (**a**) without ZPHI-method correction and (**b**) with the reflectivity corrected by the ZPHI methodology.

In this study, three *Z-R* relationships were used in combination with $R(K_{DP})$ and $R(A)$ products for rainfall estimation. In addition, two corrected horizontal reflectivity products (Z_h) were also tested. In this study, the variable Z_{h1} denotes Guaratiba's S-band radar reflectivity without the ZPHI-method correction, and Z_{h2} refers to the reflectivity corrected by the ZPHI-method attenuation. In the following, the six radar products are detailed.

1.   Product 1: $R(Z_h, K_{DP})$, Marshall–Palmer

Product 1 was generated from the application of reflectivities Z_{h1} and Z_{h2} in a hybrid algorithm, which used the *Z-R* relationship for low rainfall intensity and $R(K_{DP})$ for higher rainfall intensity. The chosen threshold reflectivity value for the algorithm was 40 dBZ, where, at usual weather radar wavelengths, strong echoes (>40 dBZ) are equivalent to convective precipitation, with stronger echoes (>60 dBZ) usually associated with hail [37]. Additionally, since the KDP becomes noisy when $Z < 40$ dBZ for S-band radar [46,62,65,66], the set value becomes a good choice.

$$R = 0.036 \cdot 10^{0.0625\ \text{dBZ}}\ for\ Z_h \leq 40\ \text{dBZ},\ \ where\ Z_h = Z_{h1}\ or\ Z_{h2}$$
$$or$$
$$R = 50.7(K_{DP})^{0.85}\ \ for\ Z_h > 40\ \text{dBZ} \tag{8}$$

The *Z-R* relationship chosen for Product 1 was the one proposed by Marshall and Palmer [45] (with parameters $a = 200$ and $b = 1.6$ in Equation (1)), which verified that stratiform precipitations followed an exponential distribution. The $R(K_{DP})$ relationship was calculated using the DSD proposed by Beard and Chuang [67] and Gu et al. [64] for determining the coefficients for S-band radar according to Figueras i Ventura et al. [27].

2. Product 2: $R(Z_h, K_{DP})$, Morales

Product 2 follows the same premises as Product 1; however, the *Z-R* relationship proposed by Morales Rodriguez [68] (with parameters $a = 378$ and $b = 1.34$ in Equation (1)) was used, which describes the DSD of convective rainfall through a Gamma function.

$$R = 0.012 \cdot 10^{0.0746 \text{ dBZ}} \; for \; Z_h \leq 40 \text{ dBZ}, \; where \; Z_h = Z_{h1} \; or \; Z_{h2}$$
$$or$$
$$R = 50.7(K_{DP})^{0.85} \; for \; Z_h > 40 \text{ dBZ}$$

(9)

3. Product 3: $R(Z_h, K_{DP})$, Pluv

Product 3 follows the premises of Product 1, but the *Z-R* relationship was obtained by determining a power function between the local measurements from the 30 rainfall stations for the five studied events and the reflectivities Z_{h1} and Z_{h2} through the least-squares method, as shown in Figure 3. The obtained *Z-R* parameters in Equation (1) were $a = 3.181$ and $b = 0.7104$ for the *Z-R* relationship with Z_{h1}, and $a = 43.583$ and $b = 0.6723$ for the *Z-R* relationship with Z_{h2}.

$$R = 0.196 \cdot 10^{0.1408 \text{ dBZ}} \; for \; Z_{h1} \leq 40 \text{ dBZ},$$
$$or$$
$$R = 50.7(K_{DP})^{0.85} \; for \; Z_{h1} > 40 \text{ dBZ}$$

(10)

and

$$R = 0.0036 \cdot 10^{0.1487 \text{ dBZ}} \; for \; Z_{h2} \leq 40 \text{ dBZ},$$
$$or$$
$$R = 50.7(K_{DP})^{0.85} \; for \; Z_{h2} > 40 \text{ dBZ}$$
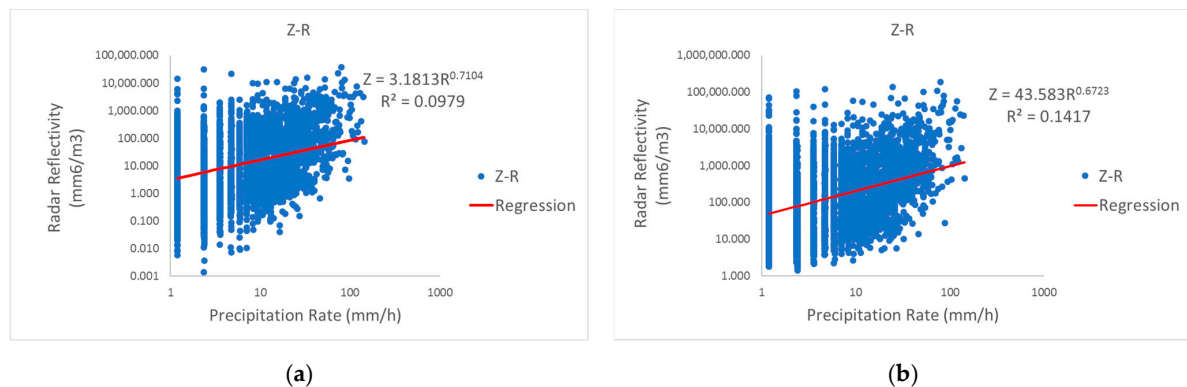
(11)

(a) (b)

Figure 3. Different regressions developed in this work between Guaratiba's S-band radar data and rain gauge measurements: (**a**) method of least squares applied to Z_{h1} (radar reflectivity without ZPHI-method correction); (**b**) method of least squares applied to Z_{h2} (radar reflectivity corrected by ZPHI methodology).

4. Product 4: $R(Z_h, A)$, Marshall—Palmer

Product 4 was obtained through the Marshall—Palmer Z-R relationship [45] (with parameters $a = 200$ and $b = 1.6$ in Equation (1)) for low rainfall intensity (≤ 40 dBZ) and the $R(A)$ relationship for higher rainfall intensity (> 40 dBZ). The $R(A)$ algorithm used by Ryzhkov et al. [53] and Wang et al. [61] was also used in this study.

$$R = 0.036 \cdot 10^{0.0625 \text{ dBZ}} \; for \; Z_h \leq 40 \text{ dBZ}, \; where \; Z_h = Z_{h1} \; or \; Z_{h2}$$
$$or$$
$$R = 4120 \cdot (A)^{1.03} \; for \; Z_h > 40 \text{ dBZ}$$

(12)

5.　Product 5: $R(Z_h, A)$, Morales Product 5 was obtained through the *Z-R* relationship proposed by Morales Rodriguez [68] (similar to Product 2, with parameters $a = 378$ and $b = 1.34$ in Equation (1)) for low rainfall intensity (≤ 40 dBZ) and the $R(A)$ relationship for higher rainfall intensity (> 40 dBZ). Similar to Product 4, the $R(A)$ algorithm used by Ryzhkov et al. [53] and Wang et al. [61] was also used in this study.

$$R = 0.012 \cdot 10^{0.0746 \text{ dBZ}} \ for \ Z_h \leq 40 \text{ dBZ}, \ where \ Z_h = Z_{h1} \ or \ Z_{h2}$$
$$or$$
$$R = 4120 \cdot (A)^{1.03} \ for \ Z_h > 40 \text{ dBZ} \tag{13}$$

6.　Product 6: $R(Z_h, A)$, Pluv Product 6 was also obtained through the *Z-R* relationship for low rainfall intensity (≤ 40 dBZ) and the $R(A)$ relationship for higher rainfall intensity (> 40 dBZ). The *Z-R* relationships were those used in Product 3. Similar to Product 4, the $R(A)$ algorithm used by Ryzhkov et al. [53] and Wang et al. [61] was also used in this study.

$$R = 0.196 \cdot 10^{0.1408 \text{ dBZ}} \ for \ Z_{h1} \leq 40 \text{ dBZ},$$
$$or$$
$$R = 4120 \cdot (A)^{1.03} \ for \ Z_{h1} > 40 \text{ dBZ} \tag{14}$$
$$and$$

$$R = 0.0036 \cdot 10^{0.1487 \text{ dBZ}} \ for \ Z_{h2} \leq 40 \text{ dBZ},$$
$$or$$
$$R = 4120 \cdot (A)^{1.03} \ for \ Z_{h2} > 40 \text{ dBZ} \tag{15}$$

2.2.3. Rainfall Events Studied

The rainfall data obtained from these stations were used to study five severe precipitation events that affected the region, spread over 17 days. The events' selection was based on the work of Alves [34], who studied the occurrence of mass movements in the city of Angra dos Reis associated with intense precipitation. Table 3 presents the studied rainfall events, the number of rain gauges used in each event, the rain gauges' and radar's temporal resolutions, and the number of radar time steps per event. In this study, only CAPPI products [37,38] at a 2 km height, generated from Guaratiba's radar data, in scans of 5 and 10 min were used.

Table 3. Rainfall events, the number of rain gauges used in each event, the rain gauges' and radar's temporal resolutions, and the number of radar time steps per event.

Event ID	Event Duration	Number of Rain Gauge Stations	Rain Gauges' Temporal Resolution	Radar's Temporal Resolution and Number of Time Steps
Event 1	14 December 2016 (00:00:00 UTC-3)–18 December 2016 (23:50:00 UTC-3)	29 [1]	10 min	10 min (720)
Event 2	21 January 2017 (00:00:00 UTC-3)–23 January 2017 (23:50:00 UTC-3)	27 [2]	10 min	10 min (227)
Event 3	13 March 2017 (00:00:00 UTC-3)–18 March 2017 (23:50:00 UTC-3)	27 [3]	10 min	10 min (720)
Event 4	12 December 2017 (00:00:00 UTC-3)–13 December 2017 (23:55:00 UTC-3)	28 [4]	10 min	5 min (275)
Event 5	3 July 2018 (00:00:00 UTC-3)–4 July 2018 (23:55:00 UTC-3)	22 [5]	10 min	5 min (201)

Notes: [1] There were no data from rain gauge P1. [2] There were no data from rain gauges P1, P11, and P29. [3] There were no data from rain gauges P11, P23, and P29. [4] There were no data from rain gauges P4 and P23. [5] There were no data from rain gauges P1, P4, P7, P12, P18, P19, P23, and P28.

2.3. Statistical Methods

To statistically analyze the comparison between the rain gauge network measurements and Guaratiba's radar data, four standard metrics were used in this study considering time series A and B, with the same number N of time steps.

1. The Root-Mean-Square Error ($RMSE$) between actual and predicted time series:

$$RMSE(A, B) = \sqrt{\frac{1}{N} \sum_i (A_i - B_i)^2} \, , \tag{16}$$

2. The Pearson correction coefficient ($Corr \in [-1, 1]$) estimates the strength and direction of the linear relationship between time series:

$$Corr(A, B) = \frac{\sum_i \left[(A_i - \overline{A}_i) \, (B_i - \overline{B}_i) \right]}{\sqrt{\sum_i (A_i - \overline{A}_i)^2} \, \sqrt{\sum_i (B_i - \overline{B}_i)^2}} \, , \tag{17}$$

3. The Nash–Sutcliffe efficiency ($Nash \in (-\infty, 1]$) measures how well the outputs of a model reproduce observations against a model that uses only the average of the observed data:

$$Nash(A, B) = 1 - \frac{\sum_i (B_i - A_i)^2}{\sum_i (B_i - \overline{B}_i)^2} \, . \tag{18}$$

4. The mean absolute error (MAE) between actual and predicted time series:

$$MAE(A, B) = \frac{1}{N} \sum_i |A_i - B_i| \, . \tag{19}$$

3. Results

In this section, a comparative analysis is carried out between the total precipitation measured at the 30 selected rain gauges located in Angra dos Reis (RJ) and the rainfall estimates computed from the different products generated with Guaratiba's S-band radar data.

3.1. Rain Gauge Data vs. Estimated Rainfall Radar Dara from Reflectivity Z_{h1}

Firstly, Figure 4 presents the total accumulated precipitation of all studied rain gauge stations and Guaratiba's six S-band radar products using Z_{h1} (radar reflectivity without ZPHI-method correction) at radar pixels where rain gauges are located for all five studied events.

In Event 1, it is observed that in the total accumulated precipitation comparison, the total rainfall estimates from Products 3 and 6 were the closest to the rain gauges' total measurements. Product 3 was closer to the rain gauges' accumulated measurements in 18 of the 29 (62.1%) active rain gauges in this event, with a mean absolute difference of 34.0% of the total accumulated precipitation (which corresponds to a mean absolute difference of 14.0 mm). Product 6 was the second-best estimator, having been the closest product to the rain gauges' accumulated measurements in 11 of the 29 (37.9%) active rain gauges, with a mean absolute difference of 44.7% of the total accumulated precipitation (corresponding to a mean absolute difference of 18.4 mm). In addition, there is a general underestimation in Products 1, 2, 4, and 5.
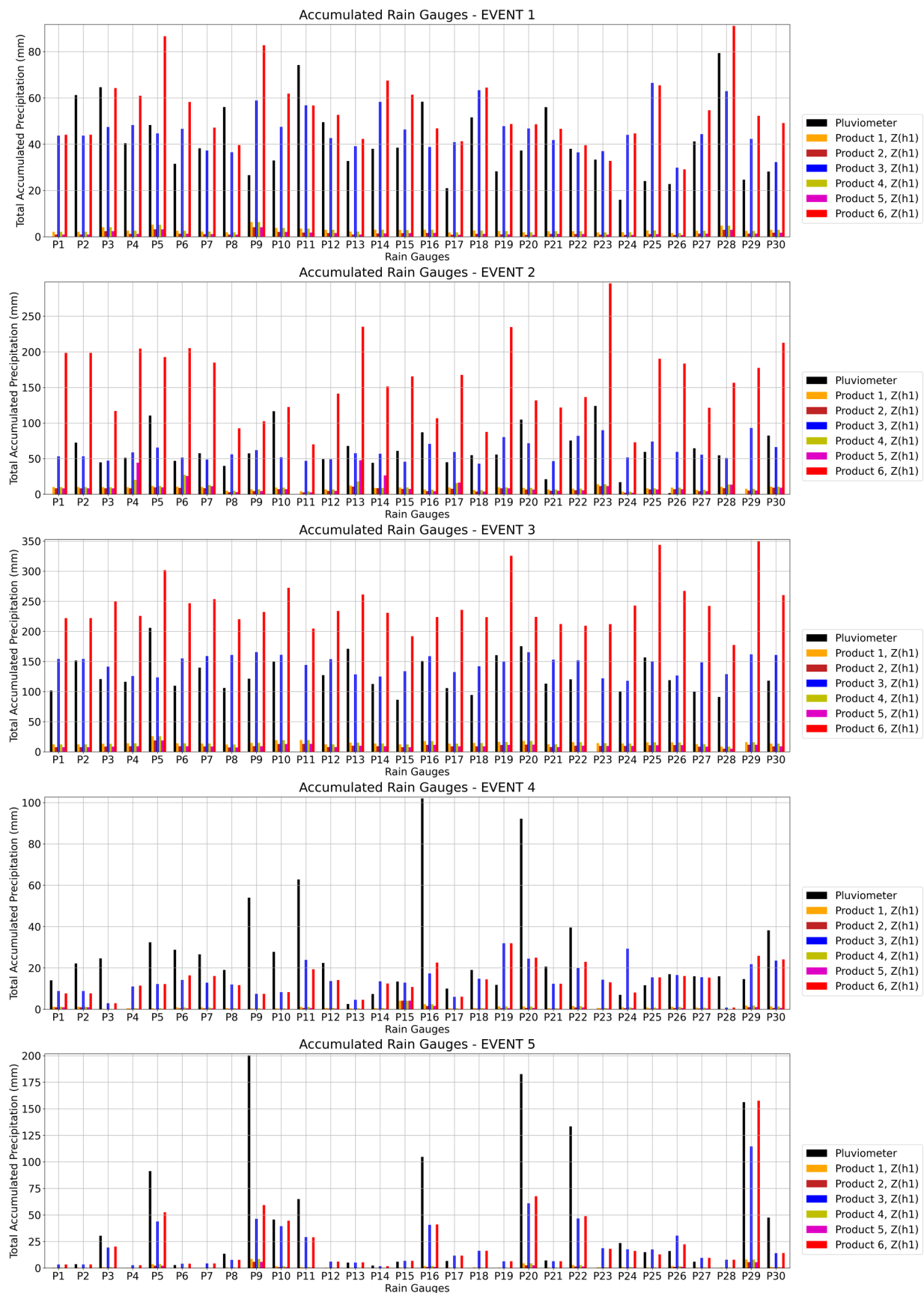
Figure 4. Total accumulated precipitation comparisons for Events 1, 2, 3, 4, and 5 between rain gauge results and Guaratiba's six S-band radar products using Z_{h1} at radar pixels where rain gauges are located.

In Event 2, Product 3 presented the best estimates when compared to the total value of the accumulated rainfall in 21 of the 27 (77.7%) active rain gauges in this event, with a mean absolute difference of 30.8% of the total accumulated precipitation (which corresponds to a mean absolute difference of 19.0 mm). In addition, similar to Event 1, Products 1, 2, 4, and 5 underestimated the rainfall when compared with the rain gauge measurements in this event. On the other hand, in this event, Product 6 considerably overestimated the rain gauge measurements.

In Event 3, Product 3 was also the one that best estimated the total accumulated rainfall values observed in all 27 of the 27 (100%) active rain gauges studied, with a mean absolute difference of 22.7% of the total accumulated precipitation (which corresponds to a mean absolute difference of 28.8 mm). In addition, similar to Events 1 and 2, Products 1, 2, 4, and 5 underestimated the rainfall when compared with the rain gauge measurements in this event. In addition, similar to Event 2, Product 6 considerably overestimated the rain gauge measurements in this event.

In Event 4, it is observed that Product 3 presented closer estimates to 14 of the 28 (50%) active rain gauges than the other Products, with a mean absolute difference of 63.4% of the total accumulated precipitation (which corresponds to a mean absolute difference of 17.5 mm), and Product 6 presented closer estimates to the other 14 of the 28 (50%) active rain gauges than the other Products, with a mean absolute difference of 60.4% of the total accumulated precipitation (corresponding to a mean absolute difference of 16.7 mm). In addition, there is an underestimation, for the most part, of all products, including Products 3 and 6 but even more pronounced for Products 1, 2, 4, and 5.

In Event 5, Product 6 presented the best estimates in 9 of the 22 (40.9%) active rain gauges, Product 3 was closer to the total accumulated measurements in 2 of the 22 (9.1%) active rain gauges, and in the other 11 of the 22 (50%) active rain gauges, both Products 3 and 6 shared the best estimates, presenting comparable values. Thus, we may say that Product 6 presented the best estimates in 20 of the 22 (90.9%) active rain gauges, with a mean absolute difference of 48.0% of the total accumulated precipitation (corresponding to a mean absolute difference of 25.4 mm). In addition, similar to Event 4, there is an underestimation, for the most part, of all products, including Products 3 and 6 but even more pronounced for Products 1, 2, 4, and 5.

Furthermore, Figure 5 presents the statistical indices (RMSE, Pearson correction coefficient, Nash–Sutcliffe efficiency, and mean absolute error) obtained from the comparison between the rainfall time series of all studied rain gauge stations and the rainfall time series obtained from Guaratiba's six S-band radar products at radar pixels where rain gauges are located for all five studied events.

In Event 1, the analyses carried out through RMSE and MAE showed that Products 1, 2, 4, and 5 performed better than Products 3 and 6; the analyses of the Corr index showed mostly similar coefficients of all products, with some important differences at a few rain gauges, and Nash index analyses showed that Products 1, 2, 4, and 5 mostly better fit the rain gauge data time series.

In Event 2, the analyses carried out through RMSE and MAE showed that Products 1, 2, 3, 4, and 5 performed better than Product 6; the analysis of the Corr index showed that Product 6 had a better correlation, with some important differences in a few rain gauges, and the analysis of the Nash index showed that Products 1, 2, 3, 4, and 5 better fit the time series of rain gauge data.

In Event 3, the analyses carried out through RMSE showed that Products 1, 2, 4, and 5 performed better than Products 3 and 6; the analysis of the Corr index showed mostly similar coefficients for all products except for Product 3, which presented worse Pearson correction coefficients than the others, and the Nash index analysis revealed that Products 1, 2, 4, and 5 better fit the time series of rain gauge data.
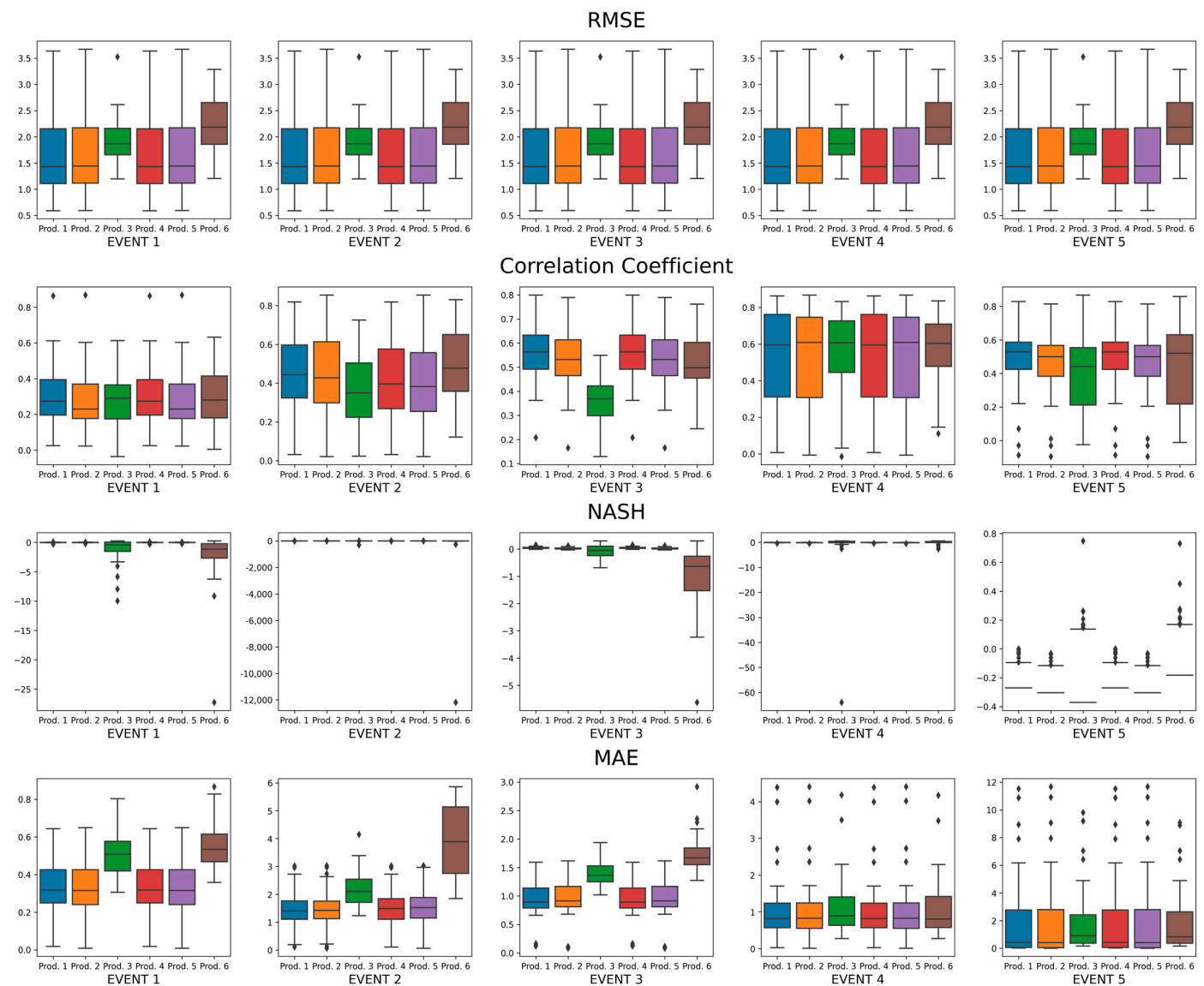
Figure 5. Statistical indices (RMSE, Pearson correction coefficient, Nash–Sutcliffe efficiency, and mean absolute error) of the comparisons for Events 1, 2, 3, 4, and 5 between rain gauge results and Guaratiba's six S-band radar products using Z_{h1} at radar pixels where rain gauges are located.

In Event 4, the analysis carried out through RMSE and MAE showed similar errors in all products; the analysis of the Corr index showed mostly similar coefficients, and the Nash index analysis also showed similarities among the products.

In Event 5, the analysis carried out through RMSE showed that Products 1, 2, 3, 4, and 5 performed better than Product 6; the analysis of MAE showed similar errors in all products; the analysis of the Corr index showed mostly similar coefficients, with some important differences in a few rain gauges, and the Nash index analysis also showed similarities among the products.

3.2. Rain Gauge Data vs. Estimated Rainfall Radar Data from Reflectivity Z_{h2}

After applying the ZPHI methodology to correct Guaratiba's S-band radar reflectivity and obtaining Z_{h2}, we reanalyzed the six radar products with this correction in all five studied events. Figure 6 presents the total accumulated precipitation of all studied rain gauge stations and Guaratiba's six S-band radar products using Z_{h2} at radar pixels where rain gauges are located.
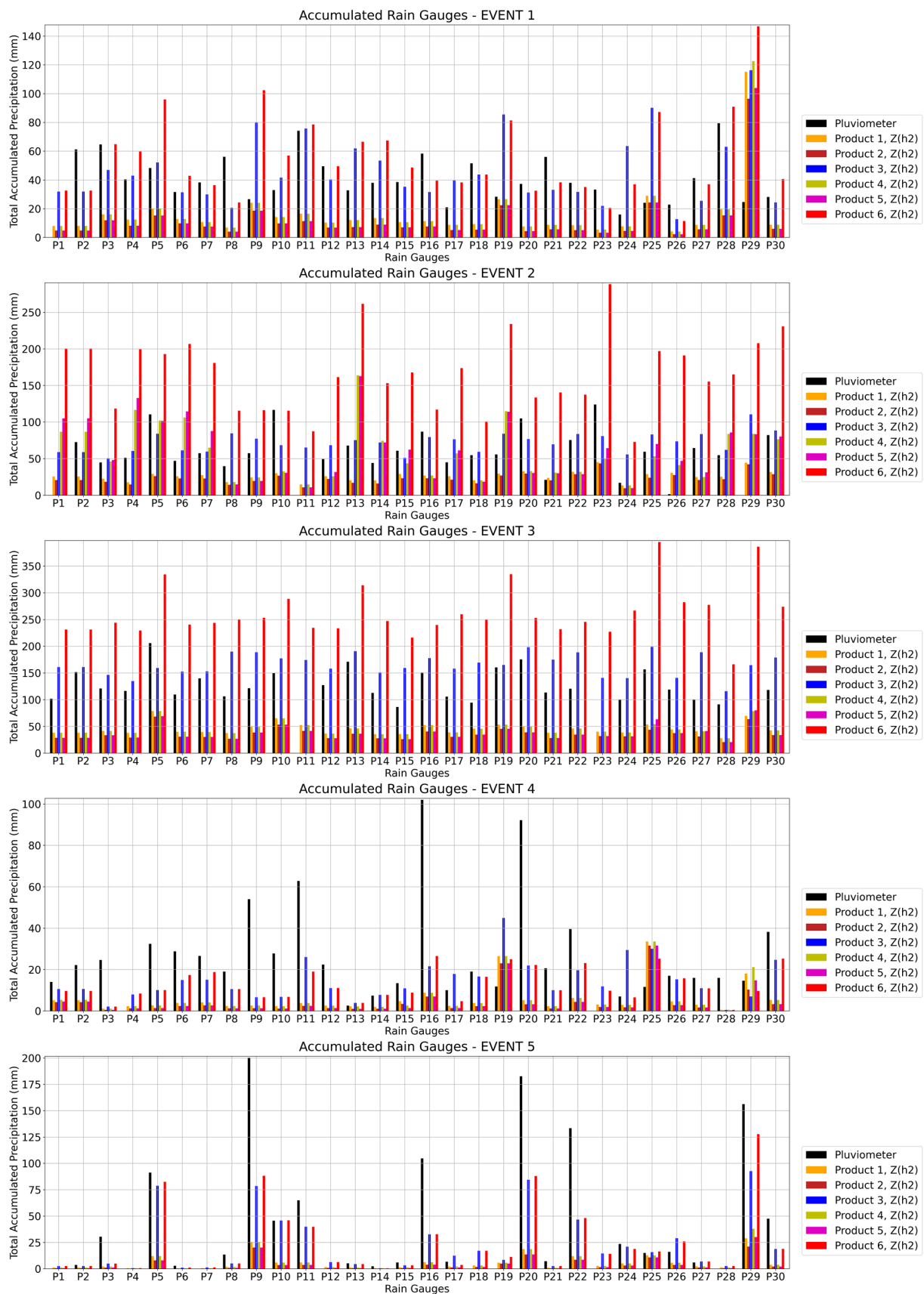
Figure 6. Total accumulated precipitation comparisons for Events 1, 2, 3, 4, and 5 between rain gauge results and Guaratiba's six S-band radar products using Z_{h2} at radar pixels where rain gauges are located.

In Event 1, it was found that the values estimated by Products 3 and 6 were the closest to the accumulated total measured by rain gauges. Product 3 was the closest in 11 of the 29 (37.9%) active rain gauges, with a mean absolute difference of 52.5% of the total accumulated precipitation for Product 3 (which corresponds to a mean absolute difference of 21.6 mm). Product 6 was the second-best estimator, being the closest product to the accumulated measurements of the rain gauges in 11 of the 29 (37.9%) active rain gauges, with an absolute mean difference of 58.6% of the total accumulated rainfall (corresponding to a mean absolute difference of 24.1 mm). Furthermore, it is evident that although there is still a general underestimation in Products 1, 2, 4, and 5, after applying the reflectivity correction by the ZPHI method, the values of these products were maximized.

In Event 2, the estimates of the total accumulated precipitation of Product 3 were the closest to the total rain gauge measurements in 13 of the 27 (48.15%) active rain gauges, with a mean absolute difference of 34.3% of the total accumulated rainfall (corresponding to a mean absolute difference of 21.2 mm). Furthermore, Products 1, 2, 4, and 5 were maximized after applying the reflectivity correction by the ZPHI method but still underestimated the rain gauge data.

In Event 3, similar to Event 2, the estimates of the total accumulated precipitation of Product 3 were the closest to the total rain gauge measurements in 23 of the 27 (85.2%) active rain gauges, with a mean absolute difference of 32.2% of the total accumulated rainfall (corresponding to a mean absolute difference of 40.9 mm). Furthermore, Products 1, 2, 4, and 5 were also maximized after applying the reflectivity correction by the ZPHI method but still underestimated the rain gauge data.

In Event 4, the estimates of the total accumulated precipitation of Product 6 were the closest to the total rain gauge measurements in 10 of the 28 (35.71%) active rain gauges, with a mean absolute difference of 60.3% of the total accumulated rainfall (corresponding to a mean absolute difference of 16.7 mm). Furthermore, Products 1, 2, 4, and 5 were also maximized after applying the reflectivity correction by the ZPHI method, getting closer to the rain gauge measurements and, in some cases, overestimating them.

In Event 5, the estimates of total accumulated precipitation of Product 6 were the closest to the total rain gauge measurements in 9 of the 22 (40.9%) active rain gauges. Product 3 was closer to the total accumulated measurements in 4 of the 22 (18.2%) active rain gauges, and in the other 8 of the 22 (36.4%) active rain gauges, both Products 3 and 6 shared the best estimates, presenting comparable values; in 1 of the 22 (4.5%) active rain gauges, both Products 1 and 4 shared the best estimates, presenting comparable values. Thus, we may say that Product 6 presented the best estimates in 17 of the 22 (77.3%) active rain gauges, with a mean absolute difference of 44.8% of the total accumulated precipitation (corresponding to a mean absolute difference of 22.7 mm). In addition, Products 1, 2, 4, and 5 were maximized after applying the reflectivity correction by the ZPHI method but still underestimated the rain gauge data.

Furthermore, Figure 7 presents the statistical indices (RMSE, Pearson correction coefficient, Nash–Sutcliffe efficiency, and mean absolute error) obtained from the comparison between the rainfall time series of all studied rain gauge stations and the rainfall time series obtained from Guaratiba's six S-band radar products at radar pixels where rain gauges are located for all the five studied events.

In Event 1, the analyses carried out using the RMSE, Corr, and Nash metrics show that all products presented similar behavior, with some important differences in a few rain gauges for Products 3 and 6. Nevertheless, when analyzing MAE estimates, it is observed that Products 1, 2, 4, and 5 present slightly better behavior than Products 3 and 6.

In Event 2, the RMSE and MAE indices showed that Products 1 and 2 performed better than Products 3, 4, 5, and 6; the analysis of the Corr index showed mostly similar coefficients for Products 1 and 2, with some important differences in a few rain gauges, and the Nash index analysis showed that Products 1, 2, 4 and 5 better fit the time series of rain gauge data.
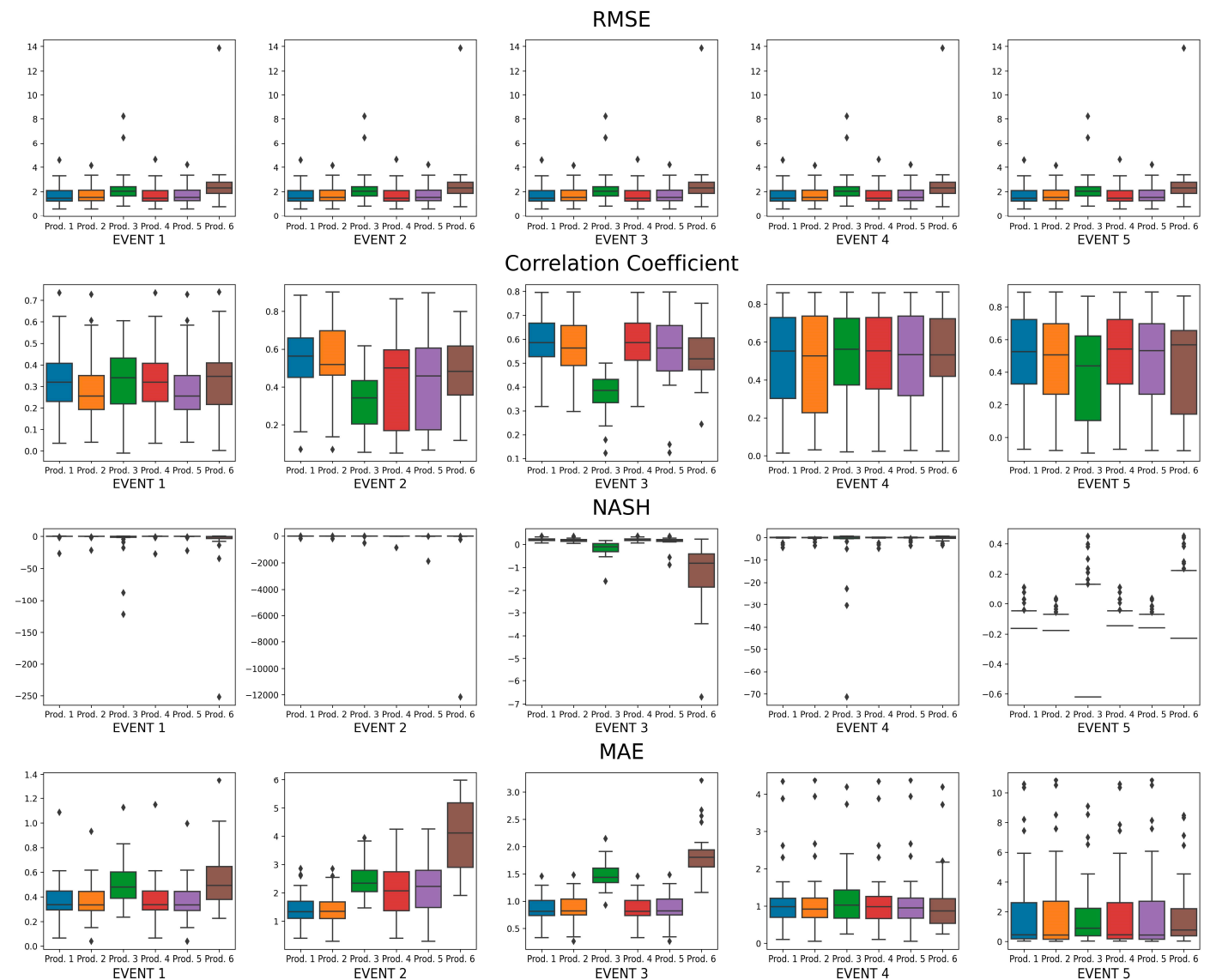
Figure 7. Statistical indices (RMSE, Pearson correction coefficient, Nash–Sutcliffe efficiency, and mean absolute error) of the comparisons for Events 1, 2, 3, 4, and 5 between rain gauge results and Guaratiba's six S-band radar products using Z_{h2} at radar pixels where rain gauges are located.

In Event 3, the RMSE and MAE indices showed that Products 1, 2, 4, and 5 performed better than Products 3 and 6; the analysis of the Corr index showed mostly similar coefficients for Products 1, 2, 4, 5, and 6 with some important differences in a few rain gauges, and the Nash index analysis showed that Products 1, 2, 4, and 5 better fit the time series of rain gauge data.

In Event 4, the RMSE and MAE indices showed that all products presented similar behavior, except for Product 3 in some rain stations; the analysis of the Corr index showed mostly similar coefficients for all products, with some important differences in a few rain gauges, and the Nash index analysis showed that Products 1, 2, 4, 5, and 6 better fit the time series of rain gauge data.

In Event 5, the analysis carried out using the RMSE, MAE, Corr, and Nash metrics shows that all products presented similar behavior, with some important differences in a few rain gauges for Products 3 and 6.

4. Discussion

The present study performed a rainfall data comparison over the municipality of Angra dos Reis, located in the state of Rio de Janeiro, Brazil. Two main data sources were used in this work: a rain gauge network with 30 pluviometric stations installed in the case study area, managed by the National Center for Monitoring and Warning of Natural Disasters (CEMADEN), and S-band radar covering the studied area operated by the Environmental State Institute of Rio de Janeiro (INEA), located in the Guaratiba neighborhood in the municipality of Rio de Janeiro (RJ), Brazil.

Weather radar estimates are affected by different factors (e.g., beam blocking, the altitude of the observation, path attenuation, the indirectness of the measurement, and distance). Many researchers have already performed comparisons between radar and rain gauges in terms of precipitation amounts [69,70]. An observed limitation of this study is the lack of a specific *Z-R* relationship for the case study area. Studies with disdrometers have been used to determine a power law function to characterize the size and velocity of precipitation particles [71], which could be carried out for this region. In this way, a region-specific *Z-R* relationship could be used to minimize the bias, especially for low radar reflectivity ($\leq$ 40 dBZ). To cope with this limitation, some *Z-R* relationships have been tested in this work. Nevertheless, in a future study, other different regression techniques could be tested to analyze the best performance of the data, including for different severe events.

In this work, six different radar data products (with and without ZPHI-method correction) were statistically compared with local rain gauge measurements by quantifying the uncertainties in precipitation estimates at radar pixels where rain gauges are located. These products combined three *Z-R* relationships (Marshall–Palmer, Morales Rodriguez, and one obtained by determining a power function between local measurements from the 30 rainfall stations for the five studied events and the radar reflectivities through the least-squares method) applied for low rainfall intensity ($\leq$ 40 dBZ) and two polarimetric S-band radar moments (K_{DP} and attenuation) for higher rainfall intensity ($>$ 40 dBZ). The proposed *Z-R* relationships were studied to identify a relationship that would better adapt to the conditions of the region, since there were no previous studies on a specific *Z-R* relationship for this locality.

The results show that the precipitation obtained from Guaratiba's S-band radar data Products 1, 2, 4, and 5 has been highly underestimated when compared with the actual rainfall values measured by local rain gauges. On the other hand, the use of the ZPHI method to correct radar reflectivity proved to be a great alternative to minimize these biases, since the reflectivity previously corrected by this method allowed the generation of more reliable rainfall estimates when compared to the rain gauge measurements.

Furthermore, it is evident in our study that the estimates computed by Products 3 and 6 are generally the best for calculating accumulated precipitation in the severe events studied when compared to the rain gauge measurements. This is because these products make use of a power law that directly relates the radar reflectivity values to the rain gauge measurements through regression techniques and therefore reduce the bias caused by the incorrect calibration of the radar.

Although the results obtained with Products 3 and 6 are better than conventional techniques at first glance, they are directly based on the spatiotemporal interval from which they were generated, increasing the error with the spatiotemporal scale or even being unusable when applied to different events. In addition, the larger the number of samples, the more difficult it is to determine a power law that can be applied with confidence in any event. Therefore, an algorithm that defines a reliable power law based on regression techniques would be needed to continuously self-adjust and have efficient tools for outlier elimination in real time. Such a model would require a high computational capacity and would be directly related to the mesh of rain gauges that would need to feed it back all the time. A sparse rain gauge network would directly increase the estimation errors. Therefore, these characteristics make these models difficult to implement in real-time

rainfall forecasting systems. Nevertheless, this will also be an issue of future work by this research group.

Finally, this work constitutes essential information for dealing with efficient regulation for rainfall monitoring and forecasting to minimize the risks associated with extreme events. This is especially important due to the significant variation in the occurrence and intensity of natural disasters associated with climate change (e.g., droughts, heatwaves, and floods) on seasonal, annual, and interdecadal scales [72–74].

Author Contributions: Conceptualization, E.J.R.d.S., C.N.A., P.C.d.O.C., R.A.A.C.e.O., M.E.S.M., J.C.C.A. and I.P.; methodology, E.J.R.d.S., C.N.A., P.C.d.O.C., R.A.A.C.e.O., M.E.S.M., J.C.C.A. and I.P.; software, E.J.R.d.S.; validation, E.J.R.d.S., C.N.A. and P.C.d.O.C.; formal analysis, E.J.R.d.S., C.N.A., P.C.d.O.C., R.A.A.C.e.O., M.E.S.M., J.C.C.A. and I.P.; investigation, E.J.R.d.S., C.N.A., P.C.d.O.C., R.A.A.C.e.O., M.E.S.M., J.C.C.A. and I.P.; resources, E.J.R.d.S., C.N.A. and P.C.d.O.C.; data curation, E.J.R.d.S. and C.N.A.; writing—original draft preparation, E.J.R.d.S., C.N.A., P.C.d.O.C., R.A.A.C.e.O., M.E.S.M., J.C.C.A. and I.P.; writing—review and editing, E.J.R.d.S., C.N.A., P.C.d.O.C., R.A.A.C.e.O., M.E.S.M., J.C.C.A. and I.P.; visualization, E.J.R.d.S., C.N.A., P.C.d.O.C., R.A.A.C.e.O., M.E.S.M., J.C.C.A. and I.P.; supervision, E.J.R.d.S., C.N.A., P.C.d.O.C., R.A.A.C.e.O., M.E.S.M., J.C.C.A. and I.P.; project administration, E.J.R.d.S., C.N.A., P.C.d.O.C., R.A.A.C.e.O., M.E.S.M., J.C.C.A. and I.P.; funding acquisition, E.J.R.d.S., C.N.A. and P.C.d.O.C. All authors have read and agreed to the published version of the manuscript.

Funding: This research was funded by CAPES (Coordenação de Aperfeiçoamento de Pessoal de Nível-Brasil), grant number 001.

Data Availability Statement: Restrictions apply to the availability of these data. Data were obatained from the Environmental State Institute of Rio de Janeiro (INEA) and the Civil Defense of the munici-pality of Angra dos Reis (RJ) and are available on request from the corresponding author with the permission of INEA and/or the Civil Defense of the municipality of Angra dos Reis (RJ).

Acknowledgments: The authors would like to thank the Environmental State Institute of Rio de Janeiro (INEA) for providing the S-band radar data and the Civil Defense of the municipality of Angra dos Reis (RJ) for providing the rain gauge network measurements.

Conflicts of Interest: The authors declare no conflict of interest.

References

1. Schmitt, T.G.; Thomas, M.; Ettrich, N. Analysis and Modeling of Flooding in Urban Drainage Systems. *J. Hydrol.* **2004**, *299*, 300–311. [CrossRef]
2. Chen, J.; Hill, A.A.; Urbano, L.D. A GIS-Based Model for Urban Flood Inundation. *J. Hydrol.* **2009**, *373*, 184–192. [CrossRef]
3. Alves De Souza, B.; Da, I.; Rocha Paz, S.; Ichiba, A.; Willinger, B.; Gires, A.; Carlos, J.; Amorim, C.; De, M.; Reis, M.; et al. Multi-Hydro Hydrological Modelling of a Complex Peri-Urban Catchment with Storage Basins Comparing C-Band and X-Band Radar Rainfall Data. *Hydrol. Sci. J.* **2018**, *63*, 1619–1635. [CrossRef]
4. Celebrini De Oliveira Campos, P.; Da, T.; Rocha Paz, S.; Lenz, L.; Qiu, Y.; Alves, C.N.; Paula, A.; Simoni, R.; Carlos, J.; Amorim, C.; et al. Multi-Criteria Decision Method for Sustainable Watercourse Management in Urban Areas. *Sustainability* **2020**, *12*, 6493. [CrossRef]
5. Qiu, Y.; Da Silva Rocha Paz, I.; Chen, F.; Versini, P.A.; Schertzer, D.; Tchiguirinskaia, I. Space Variability Impacts on Hydrological Responses of Nature-Based Solutions and the Resulting Uncertainty: A Case Study of Guyancourt (France). *Hydrol. Earth Syst. Sci.* **2021**, *25*, 3137–3162. [CrossRef]
6. Loukas, A.; Llasat, M.C.; Ulbrich, U. Preface "Extreme Events Induced by Weather and Climate Change: Evaluation, Forecasting and Proactive Planning. *Nat. Hazards Earth Syst. Sci.* **2010**, *10*, 1895–1897. [CrossRef]
7. Pumo, D.; Arnone, E.; Francipane, A.; Caracciolo, D.; Noto, L.V. Potential Implications of Climate Change and Urbanization on Watershed Hydrology. *J. Hydrol.* **2017**, *554*, 80–99. [CrossRef]
8. Arnone, E.; Pumo, D.; Francipane, A.; La Loggia, G.; Noto, L.V. The Role of Urban Growth, Climate Change, and Their Interplay in Altering Runoff Extremes. *Hydrol. Process.* **2018**, *32*, 1755–1770. [CrossRef]
9. Borges, E.C.; Paz, I.; Leite Neto, A.D.; Willinger, B.; Ichiba, A.; Gires, A.; de Campos, P.C.O.; Monier, L.; Cardinal, H.; Amorim, J.C.C.; et al. Evaluation of the Spatial Variability of Ecosystem Services and Natural Capital: The Urban Land Cover Change Impacts on Carbon Stocks. *Int. J. Sustain. Dev. World Ecol.* **2020**, *28*, 339–349. [CrossRef]
10. Felix, N.B.; de Campos, P.C.O.; Paz, I.; Marques, M.E.S. Geoprocessing Applied to the Assessment of Carbon Storage and Sequestration in a Brazilian Medium-Sized City. *Sustain.* **2022**, *14*, 8761. [CrossRef]

11. Ochoa-Rodriguez, S.; Wang, L.P.; Gires, A.; Pina, R.D.; Reinoso-Rondinel, R.; Bruni, G.; Ichiba, A.; Gaitan, S.; Cristiano, E.; Van Assel, J.; et al. Impact of Spatial and Temporal Resolution of Rainfall Inputs on Urban Hydrodynamic Modelling Outputs: A Multi-Catchment Investigation. *J. Hydrol.* **2015**, *531*, 389–407. [CrossRef]

12. Paz, I.; Willinger, B.; Gires, A.; de Souza, B.A.; Monier, L.; Cardinal, H.; Tisserand, B.; Tchiguirinskaia, I.; Schertzer, D. Small-Scale Rainfall Variability Impacts Analyzed by Fully-Distributed Model Using C-Band and X-Band Radar Data. *Water* **2019**, *11*, 1273. [CrossRef]

13. Lee, J.; Paz, I.; Schertzer, D.; Lee, D.I.; Tchiguirinskaia, I. Multifractal Analysis of Rainfall-Rate Datasets Obtained by Radar and Numerical Model: The Case Study of Typhoon Bolaven (2012). *J. Appl. Meteorol. Climatol.* **2020**, *59*, 819–840. [CrossRef]

14. Cole, S.J.; Moore, R.J. Hydrological Modelling Using Raingauge- and Radar-Based Estimators of Areal Rainfall. *J. Hydrol.* **2008**, *358*, 159–181. [CrossRef]

15. Ochoa-Rodriguez, S.; Wang, L.P.; Willems, P.; Onof, C. A Review of Radar-Rain Gauge Data Merging Methods and Their Potential for Urban Hydrological Applications. *Water Resour. Res.* **2019**, *55*, 6356–6391. [CrossRef]

16. Del Giudice, D.; Honti, M.; Scheidegger, A.; Albert, C.; Reichert, P.; Rieckermann, J. Improving Uncertainty Estimation in Urban Hydrological Modeling by Statistically Describing Bias. *Hydrol. Earth Syst. Sci.* **2013**, *17*, 4209–4225. [CrossRef]

17. Paz, I.; Willinger, B.; Gires, A.; Ichiba, A.; Monier, L.; Zobrist, C.; Tisserand, B.; Tchiguirinskaia, I.; Schertzer, D. Multifractal Comparison of Reflectivity and Polarimetric Rainfall Data from C- and X-Band Radars and Respective Hydrological Responses of a Complex Catchment Model. *Water* **2018**, *10*, 269. [CrossRef]

18. Orellana-Alvear, J.; Célleri, R.; Rollenbeck, R.; Bendix, J. Optimization of X-Band Radar Rainfall Retrieval in the Southern Andes of Ecuador Using a Random Forest Model. *Remote Sens.* **2019**, *11*, 1632. [CrossRef]

19. de Oliveira Campos, P.C.; Paz, I. Spatial Diagnosis of Rain Gauges' Distribution and Flood Impacts: Case Study in Itaperuna, Rio de Janeiro—Brazil. *Water* **2020**, *12*, 1120. [CrossRef]

20. Villarini, G.; Smith, J.A.; Lynn Baeck, M.; Sturdevant-Rees, P.; Krajewski, W.F. Radar Analyses of Extreme Rainfall and Flooding in Urban Drainage Basins. *J. Hydrol.* **2010**, *381*, 266–286. [CrossRef]

21. Orellana-Alvear, J.; Célleri, R.; Rollenbeck, R.; Muñoz, P.; Contreras, P.; Bendix, J. Assessment of Native Radar Reflectivity and Radar Rainfall Estimates for Discharge Forecasting in Mountain Catchments with a Random Forest Model. *Remote Sens.* **2020**, *12*, 1986. [CrossRef]

22. Paz, I.; Tchiguirinskaia, I.; Schertzer, D. Rain Gauge Networks' Limitations and the Implications to Hydrological Modelling Highlighted with a X-Band Radar. *J. Hydrol.* **2020**, *583*, 124615. [CrossRef]

23. Krajewski, W.F.; Villarini, G.; Smith, J.A. RADAR-Rainfall Uncertainties: Where Are We after Thirty Years of Effort? *Bull. Am. Meteorol. Soc.* **2010**, *91*, 87–94. [CrossRef]

24. Thorndahl, S.; Nielsen, J.E.; Rasmussen, M.R. Bias Adjustment and Advection Interpolation of Long-Term High Resolution Radar Rainfall Series. *J. Hydrol.* **2014**, *508*, 214–226. [CrossRef]

25. Bringi, V.N.; Chandrasekar, V. *Polarimetric Doppler Weather Radar: Principles and Applications*; Cambridge University Press: Cambridge, UK, 2001. [CrossRef]

26. Illingworth, A.J.; Blackman, T.M. The Need to Represent Raindrop Size Spectra as Normalized Gamma Distributions for the Interpretation of Polarization Radar Observations. *J. Appl. Meteorol.* **2002**, *41*, 286–297. [CrossRef]

27. Figueras i Ventura, J.; Boumahmoud, A.-A.; Fradon, B.; Dupuy, P.; Tabary, P. Long-Term Monitoring of French Polarimetric Radar Data Quality and Evaluation of Several Polarimetric Quantitative Precipitation Estimators in Ideal Conditions for Operational Implementation at C-Band. *Q. J. R. Meteorol. Soc.* **2012**, *138*, 2212–2228. [CrossRef]

28. Chandrasekar, V.; Baldini, L.; Bharadwaj, N.; Smith, P.L. Calibration Procedures for Global Precipitation-Measurement Ground-Validation Radars | URSI Journals & Magazine | IEEE Xplore. *URSI Radio Sci. Bull. l.* **2015**, *355*, 45–73. [CrossRef]

29. Hall, W.; Rico-Ramirez, M.A.; Krämer, S. Classification and Correction of the Bright Band Using an Operational C-Band Polarimetric Radar. *J. Hydrol.* **2015**, *531*, 248–258. [CrossRef]

30. INEA—Instituto Estadual de Ambiente. Monitoramento Hidrometeorológico. Available online: http://www.inea.rj.gov.br/ar-agua-e-solo/monitoramento-hidrometeorologico/ (accessed on 7 October 2022).

31. IBGE—Instituto Brasileiro de Geografia e Estatística. Portal IBGE Cidades. Available online: https://cidades.ibge.gov.br/brasil/rj/angra-dos-reis/panorama (accessed on 5 October 2022).

32. DRM. Carta Geotécnica de Aptidão Urbana-Relatório Consolidado Do Município de Angra Dos Reis. Available online: http://www.drm.rj.gov.br/ (accessed on 11 October 2022).

33. DRM-RJ/CPRM. Geologia, Geomorfologia, Geoquímica, Geofísica, Recusos Minerais, Economia Mineral, Hidrogeologia, Estudos de Chuvas Intensas, Aptidão Agrícola, Uso e Cobertura Do Solo, Inventário de Escorregamentos, Diagnóstico Geoambiental. Rio de Janeiro. CPRM: Embrapa Solos: DRM-RJ. Available online: http://www.cprm.gov.br/publique/Gestao-Territorial/Geologia%2C-Meio-Ambiente-e-Saude/Projeto-Rio-de-Janeiro-3498.html (accessed on 11 October 2022).

34. Alves, C.N. *Previsão de Deslizamento de Encostas a Partir de Modelagem Com Base Física: Estudo de Caso No Município de Angra Dos Reis, Rio de Janeiro*; Instituto Militar de Engenharia: Rio de Janeiro, Brazil, 2020.

35. da Paz, T.S.R.; da Rocha Junior, V.G.; de Campos, P.C.O.; Paz, I.; Caiado, R.G.G.; de Rocha, A.A.; Lima, G.B.A. Hybrid Method to Guide Sustainable Initiatives in Higher Education: A Critical Analysis of Brazilian Municipalities. *Int. J. Sustain. High. Educ.* **2022**, *ahead-of-print*. [CrossRef]

36. WMO. *Guide to Instruments and Methods of Observation (WMO-No. 8)*; WMO: Geneva, Switzerland, 2018; Volume I & II, ISBN 978-92-63-10008-5.

37. Fabry, F. *Radar Meteorology: Principles and Practice*; Cambridge University Press: Cambridge, UK, 2015; pp. 1–256. [CrossRef]

38. Rauber, R.M.; Nesbitt, S.W. *Radar Meteorology: A First Course*; Wiley Blackwell: Hoboken, NJ, USA, 2016; ISBN 9781118432662.

39. Barnes, S.L. A Technique for Maximizing Details in Numerical Weather Map Analysis. *J. Appl. Meteorol.* **1964**, *3*, 396–409. [CrossRef]

40. Pauley, P.M.; Wu, X. The Theoretical, Discrete, and Actual Response of the Barnes Objective Analysis Scheme for One- and Two-Dimensional Fields. *Mon. Weather Rev.* **1990**, *118*, 1145–1164. [CrossRef]

41. Helmus, J.J.; Collis, S.M. The Python ARM Radar Toolkit (Py-ART), a Library for Working with Weather Radar Data in the Python Programming Language. *J. Open Res. Softw.* **2016**, *4*, 25. [CrossRef]

42. CRESSMAN, G.P. AN OPERATIONAL OBJECTIVE ANALYSIS SYSTEM. *Mon. Weather Rev.* **1959**, *87*, 367–374. [CrossRef]

43. Askelson, M.A.; Aubagnac, J.P.; Straka, J.M. An Adaptation of the Barnes Filter Applied to the Objective Analysis of Radar Data. *Mon. Weather Rev.* **2000**, *128*, 3050–3082. [CrossRef]

44. Zürcher, B.K. Fast Barnes Interpolation. *Geosci. Model Dev. Discuss.* **2022**. [CrossRef]

45. Marshall, J.S.; Palmer, W.M.K. The Distribution of Raindrops with Size. *J. Meteorol.* **1948**, *5*, 165–166. [CrossRef]

46. Ryzhkov, A.; Zrnić, D.; Atlas, D. Polarimetrically Tuned R (Z) Relations and Comparison of Radar Rainfall Methods. *J. Appl. Meteorol.* **1997**, *36*, 340–349. [CrossRef]

47. Ryzhkov, A.; Zhang, P.; Bukovčić, P.; Zhang, J.; Cocks, S. Polarimetric Radar Quantitative Precipitation Estimation. *Remote Sens.* **2022**, *14*, 1695. [CrossRef]

48. Orellana-Alvear, J.; Célleri, R.; Rollenbeck, R.; Bendix, J. Analysis of Rain Types and Their Z–R Relationships at Different Locations in the High Andes of Southern Ecuador. *J. Appl. Meteorol. Climatol.* **2017**, *56*, 3065–3080. [CrossRef]

49. Seliga, T.A.; Bringi, V.N. Potential Use of Radar Differential Reflectivity Measurements at Orthogonal Polarizations for Measuring Precipitation. *J. Appl. Meteorol. Climatol.* **1976**, *15*, 69–76. [CrossRef]

50. Seo, B.C.; Krajewski, W.F.; Ryzhkov, A. Evaluation of the Specific Attenuation Method for Radar-Based Quantitative Precipitation Estimation: Improvements and Practical Challenges. *J. Hydrometeor.* **2020**, *21*, 1333–1347. [CrossRef]

51. Wijayarathne, D.; Boodoo, S.; Coulibaly, P.; Sills, D. Evaluation of Radar Quantitative Precipitation Estimates (QPEs) as an Input of Hydrological Models for Hydrometeorological Applications. *J. Hydrometeor.* **2020**, *21*, 1847–1864. [CrossRef]

52. Cifelli, R.; Chandrasekar, V.; Lim, S.; Kennedy, P.C.; Wang, Y.; Rutledge, S.A. A New Dual-Polarization Radar Rainfall Algorithm: Application in Colorado Precipitation Events. *J. Atmos. Ocean. Technol.* **2011**, *28*, 352–364. [CrossRef]

53. Ryzhkov, A.; Diederich, M.; Zhang, P.; Simmer, C. Potential Utilization of Specific Attenuation for Rainfall Estimation, Mitigation of Partial Beam Blockage, and Radar Networking. *J. Atmos. Ocean. Technol.* **2014**, *31*, 599–619. [CrossRef]

54. Maesaka, T.; Iwanami, K.; Maki, M. Non-Negative KDP Estimation by Monotone Increasing PHIDP Assumption below Melting Layer. *Seventh Eur. Conf. Radar Meteorol. Hydrol.* 2012, p. 2012. Available online: http://www.meteo.fr/cic/meetings/2012/ERAD/extended_abs/QPE_233_ext_abs.pdf (accessed on 1 November 2022).

55. Maesaka, T. Operational Rainfall Estimation by X-Band MP Radar Network in MLIT, Japan. In Proceedings of the 35th Conference on Radar Meteorology, Pittsburgh, PA, USA, 26–30 September 2011.

56. Ryzhkov, A.V.; Zrnic, D.S. *Radar Polarimetry for Weather Observations*; *Springer Atmospheric Sciences*, 1st ed.; Springer International Publishing: Cham, Switzerland, 2019; ISBN 978-3-030-05092-4.

57. Cocks, S.B.; Tang, L.; Zhang, P.; Ryzhkov, A.; Kaney, B.; Elmore, K.L.; Wang, Y.; Zhang, J.; Howard, K. A Prototype Quantitative Precipitation Estimation Algorithm for Operational S-Band Polarimetric Radar Utilizing Specific Attenuation and Specific Differential Phase. Part II: Performance Verification and Case Study Analysis. *J. Hydrometeor.* **2019**, *20*, 999–1014. [CrossRef]

58. Testud, J.; Le Bouar, E.; Obligis, E.; Ali-Mehenni, M. The Rain Profiling Algorithm Applied to Polarimetric Weather Radar. *J. Atmos. Ocean. Technol.* **2000**, *17*, 332–356. [CrossRef]

59. Tabary, P.; Boumahmoud, A.A.; Andrieu, H.; Thompson, R.J.; Illingworth, A.J.; Bouar, E.L.; Testud, J. Evaluation of Two " Integrated" Polarimetric Quantitative Precipitation Estimation (QPE) Algorithms at C-Band. *J. Hydrol.* **2011**, *405*, 248–260. [CrossRef]

60. Le Bouar, E.; Testud, J.; Keenan, T.D. Validation of the Rain Profiling Algorithm "ZPHI" from the C-Band Polarimetric Weather Radar in Darwin. *J. Atmos. Ocean. Technol.* **2001**, *18*, 1819–1837. [CrossRef]

61. Wang, Y.; Zhang, P.; Ryzhkov, A.V.; Zhang, J.; Chang, P.L. Utilization of Specific Attenuation for Tropical Rainfall Estimation in Complex Terrain. *J. Hydrometeor.* **2014**, *15*, 2250–2266. [CrossRef]

62. A-si, Z.; Chao-ying, U.; Shengo, C.; Peng-fei, Z.; Dong-ming, H.; Liu-si, X. Utilization of Specific Attenuation for Rainfall Estimation in Southern China. *J. Trop. Meteorol.* **2020**, *26*, 48–61. [CrossRef]

63. Wang, Y.; Cocks, S.; Tang, L.; Ryzhkov, A.; Zhang, P.; Zhang, J.; Howard, K. A Prototype Quantitative Precipitation Estimation Algorithm for Operational S-Band Polarimetric Radar Utilizing Specific Attenuation and Specific Differential Phase. Part I: Algorithm Description. *J. Hydrometeor.* **2019**, *20*, 985–997. [CrossRef]

64. Gu, J.Y.; Ryzhkov, A.; Zhang, P.; Neilley, P.; Knight, M.; Wolf, B.; Lee, D.I. Polarimetric Attenuation Correction in Heavy Rain at C Band. *J. Appl. Meteorol. Climatol.* **2011**, *50*, 39–58. [CrossRef]

65. Ryzhkov, A.; Zrnić, D. Assessment of Rainfall Measurement That Uses Specific Differential Phase. *J. Appl. Meteorol.* **1996**, *35*, 2080–2090. [CrossRef]

66.   Ryzhkov, A.V.; Giangrande, S.E.; Melnikov, V.M.; Schuur, T.J. Calibration Issues of Dual-Polarization Radar Measurements. *J. Atmos. Ocean. Technol.* **2005**, *22*, 1138–1155. [CrossRef]

67.   Beard, K.V.; Chuang, C. A New Model for the Equilibrium Shape of Raindrops. *J. Atmos. Sci.* **1987**, *44*, 1509–1524. [CrossRef]

68.   Morales, C.A.R. *Distribuição de Tamanho de Gotas de Chuva Nos Trópicos: Ajuste de Uma Função Gamma e Aplicações*; Universidade de São Paulo: Sao Paulo, Brazil, 1991.

69.   Sebastianelli, S.; Russo, F.; Adirosi, E.; Napolitano, F.; Baldini, L. A Test Bed for Verification of a Methodology to Correct the Effects of Range Dependent Errors on Radar Estimates. Proceeding of the 7th European Conf. Radar Meteorology and Hydrology, Météo France, Toulouse, France, 24–29 June 2012.

70.   Di Curzio, D.; Di Giovanni, A.; Lidori, R.; Montopoli, M.; Rusi, S. Comparing Rain Gauge and Weather Radar Data in the Estimation of the Pluviometric Inflow from the Apennine Ridge to the Adriatic Coast (Abruzzo Region-Central Italy). 2022. Available online: https://www.preprints.org/manuscript/202211.0051 (accessed on 1 November 2022). [CrossRef]

71.   Gires, A.; Tchiguirinskaia, I.; Schertzer, D. Pseudo-Radar Algorithms with Two Extremely Wet Months of Disdrometer Data in the Paris Area. *Atmos. Res.* **2018**, *203*, 216–230. [CrossRef]

72.   Mie Sein, Z.M.; Ullah, I.; Saleem, F.; Zhi, X.; Syed, S.; Azam, K. Interdecadal Variability in Myanmar Rainfall in the Monsoon Season (May–October) Using Eigen Methods. *Water* **2021**, *13*, 729. [CrossRef]

73.   Ullah, I.; Saleem, F.; Iyakaremye, V.; Yin, J.; Ma, X.; Syed, S.; Hina, S.; Asfaw, T.G.; Omer, A. Projected Changes in Socioeconomic Exposure to Heatwaves in South Asia Under Changing Climate. *Earth's Futur.* **2022**, *10*, e2021EF002240. [CrossRef]

74.   Ullah, I.; Ma, X.; Asfaw, T.G.; Yin, J.; Iyakaremye, V.; Saleem, F.; Xing, Y.; Azam, K.; Syed, S. Projected Changes in Increased Drought Risks Over South Asia Under a Warmer Climate. *Earth's Futur.* **2022**, *10*, e2022EF002830. [CrossRef]